Materials Research Express

PAPER

Synthesis of transition metal dichalcogenides and their heterostructures

Materials Research Express

PAPER

Synthesis of transition metal dichalcogenides and their heterostructures

RECEIVED
21 June 2018

REVISED
19 July 2018

ACCEPTED FOR PUBLICATION
9 August 2018

PUBLISHED
17 August 2018

Yuhang Cai, Kai Xu and Wenjuan Zhu[1]

Department of Electrical and Computer Engineering, University of Illinois at Urbana-Champaign, Urbana, IL 61801, United States of America

[1] Author to whom any correspondence should be addressed

E-mail: wjzhu@illinois.edu

Keywords: transition metal dichalcogenide, lateral heterostructure, sapphire substrate, MoS_2, WSe_2

Abstract

As compared to the heterostructures based on bulk materials, the heterostructures based on transition metal dichalcogenides (TMDCs) have the advantages of atomically sharp hetero-interface and freedom from lattice-match restriction, which make them promising for nanoscale electronic and photonic devices. In this paper, we systematically investigate the synthesis of TMDC heterostructures using two-step processes via chemical vapor deposition (CVD). We found that if a MoS_2 growth at 730 °C is followed by a WSe_2 growth at 875 °C, the selenium atoms in the precursor will replace the sulfur atoms in MoS_2 during the second step and form $MoSe_2/WSe_2$ lateral heterostructures. On the other hand, if WSe_2 growth is followed by MoS_2 growth, WSe_2/MoS_2 lateral heterostructures were formed and no ion-exchange was observed. This result indicates that in the two-step processes, low-temperature growth followed by high-temperature growth may result in ion-exchange in the first material, while high-temperature growth followed by low-temperature growth results in epitaxy growth along the edge without ion-exchange. In addition, we have investigated the synthesis of MoS_2 and WSe_2 on sapphire substrates. In contrast to MoS_2 grown on SiO_2/Si substrates where the domains are randomly oriented, the domain edges of MoS_2 grown on sapphire substrates are mostly aligned to the primary directions, which can significantly reduce the amount of grain boundaries when the domains are merged together to form continuous films. This finding will be critical to enable the fabrication of large-scale electronic devices with high-performance and uniform distributions across the wafers based on these materials.

1. Introduction

Heterostructures and superlattices are important building blocks for electronic and photonic devices, including tunneling field-effect transistors, tunneling diodes, lasers, photodetectors and solar cells [1–9]. Traditionally, heterostructures are based on bulk materials fabricated by epitaxy growth. However, due to the covalent bonding between atoms at the hetero-interface, the choice of materials is limited by the lattice-match requirement. Transition metal dichalcogenides (TMDCs) emerged in recent years as a new group of materials for heterostructures. Since the individual TMDC layers are all held by weak van der Waals forces, the choice of materials is no longer limited by the lattice-match. In addition, these TMDC heterostructures can provide atomically sharp interface, which is another advantage as compared to traditional 3D bulk heterostructures [10].

There are several techniques that can form TMDC heterostructures. The first method is mechanical exfoliation and stacking. Using this method, a large variety of heterostructures were constructed. However, the thickness, size and location of the exfoliated flakes are difficult to control. The second method is to transfer TMDC monolayers grown by CVD and stack them to form TMDC heterostructures. In this approach, polymethyl methacrylate (PMMA) is usually spun on the TMDC layers to serve as a supporting layer, while potassium hydroxide (KOH) is used to release the TMDC layers from the SiO_2/Si substrate. Then two different

TMDC layers are stacked together using aligned transfer technique under microscope. A variety of TMDC heterostructures have been made using this method [10–17]. This method is very convenient to form vertical heterostructures, but it is difficult to make lateral heterostructures, which requires atomic stitching at the boundary. The third method is growing TMDC heterostructures by CVD. It is reported that lateral $MoSe_2/WSe_2$ heterostructures can be synthesized via a one-step physical vapor transport (PVT) process using a mixture of $MoSe_2$ and WSe_2 precursors. Since $MoSe_2$ evaporates more rapidly than WSe_2, $MoSe_2$ triangles are formed on the substrate at the initial stage. As the $MoSe_2$ precursor runs out, a WSe_2 film would then start to grow on the substrate [18]. A similar one-step process was also reported for MoS_2/WS_2 heterostructure growth, where a mixture of MoO_3, tungsten, sulfur and tellurium precursors were used [19]. The difference in the nucleation and growth rate gives rise the sequential growth of MoS_2 and WS_2, instead of $Mo_xW_{1-x}S_2$ alloy [19]. However, for the lateral heterostructures grown by the one-step process, it is difficult to control the size of each material. In addition, since the precursors for both materials co-exist in the chamber, it is very challenging to avoid intermixing of the two materials and achieve an atomically sharp interface in the lateral heterostructures when using this method. Alternatively, two-step growth was investigated and CVD MoS_2/WS_2, $WSe_2/MoSe_2$, and WSe_2/MoS_2 heterostructures were fabricated using this method [20–23]. In this paper, we propose a new method to grow TMDC heterostructure: two-step growth with ion-exchange. We found that when MoS_2 was grown at 730 °C followed by WSe_2 growth at 875 °C, the sulfur atom in the MoS_2 was replaced by the selenium atom in the subsequent growth. As a result, lateral $MoSe_2/WSe_2$ heterostructures were formed. When we reversed the growth sequence, growing WSe_2 first at 875 °C followed by MoS_2 growth at 730 °C, no ion-exchange was observed and lateral WSe_2/MoS_2 heterostructures were formed. In addition, we also investigated the MoS_2 and WSe_2 growth on sapphire substrates. We found that the domain edges of MoS_2 grown on sapphire are highly oriented while those of WSe_2 grown on sapphire are mostly oriented randomly.

2. Results and discussions

2.1. CVD MoS_2 and WSe_2 on SiO_2/Si substrate

Large-scale monolayer MoS_2 was synthesized by atmosphere pressure CVD (APCVD) using a three-zone furnace. Perylene-3, 4, 9, 10-tetracarboxylic acid tetra-potassium salt (PTAS) seeding promoter (100 mg L^{-1}) was put on the clean 280 nm SiO_2/Si substrate treated by piranha solution. Sulfur powder (0.40 g) was loaded in the first zone and MoO_3 powder (0.06 g) was placed in the middle zone of the furnace. Argon (Ar) gas was used as the carrier gas, and a flow rate of 486 standard cubic centimeters per minute (sccm) was used during the growth. The temperature in the second zone was set at 730 °C while the temperature for first zone was set at 200 °C during growth. The growth duration is 5 min. Large-area of MoS_2 with continuous coverage was obtained, shown in figure 1(a). The size of the continuous film can reach several millimeters. At the edge of the continuous film, individual triangles were visible. Figure 1(b) shows an optical image of an individual MoS_2 triangle. The domain size of the MoS_2 triangle can reach 80 μm. Photoluminescence (PL), Raman spectrum, and atomic force microscopy (AFM) were carried out on these films, shown in figures 1(c)–(f). A 532 nm laser was used as an excitation source in Raman and PL measurements. A bright light emission at ~1.83 eV and a symmetrical single PL peak suggest the direct band gap nature of monolayer MoS_2, showing good agreement with other recent reports about PL of monolayer MoS_2 [24–26]. The peak of the Raman spectrum located at 385 and 405 cm^{-1} corresponds to the E' and A_1' modes of MoS_2 [27]. Comparing the peak position with the spectrum obtained from the exfoliated monolayer MoS_2 [28], we verify that the MoS_2 film is monolayer. The AFM image shows a clear triangle pattern. From the AFM step height profile, a thickness of ~0.8 nm is extracted, confirming its monolayer character.

Different from the growth of MoS_2, monolayer WSe_2 were synthesized using a single-zone furnace with hydrogen (H_2) gas. Tungsten oxide (WO_3) powder was put in the central part of the furnace, where the temperature is set as 875 °C, and selenium powder was placed at the edge of the hot zone, which is about 10 cm away from the WO_3 precursor. The selenium vapor was carried into the hot zone by the mixture of 100 sccm Ar and 30 sccm H_2. The SiO_2/Si wafers were put on top of the WO_3 crucible, facing down. We have investigated various growth temperatures (from 825 °C to 975 °C) and growth durations (from 5 min to 12 min), and found that WSe_2 grown at 875 °C for 6 min has the best morphology. Under this growth condition, monolayer WSe_2 films with domain size up to 120 μm were synthesized, shown in figure 2(a). A strong PL peak at around 1.61 eV was observed in the PL spectrum (figure 2(b)), indicating the film is monolayer WSe_2 [29–35]. In the Raman spectrum (figure 2(c)), the peaks at 250.9 and 260.6 cm^{-1} correspond to the E' and A_1' modes of WSe_2 respectively [36]. The AFM image is shown in figure 2(d) and the height profile is shown in the inset of figure 2(d), which further confirms that the WSe_2 film is monolayer.

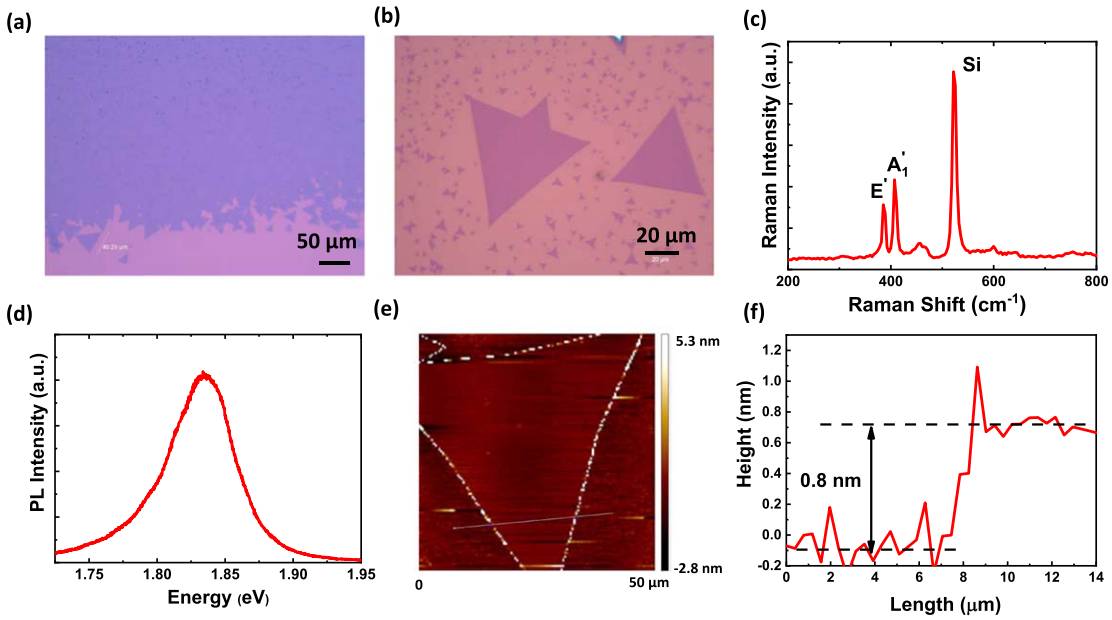

Figure 1. Microscopic characterization of monolayer MoS_2 grown by CVD. (a) Optical image of a continuous MoS_2 film. (b) Optical image of an individual MoS_2 triangle. (c) Raman spectrum, (d) Photoluminescence, (e) AFM image, and (f) AFM height profile of the monolayer MoS_2.

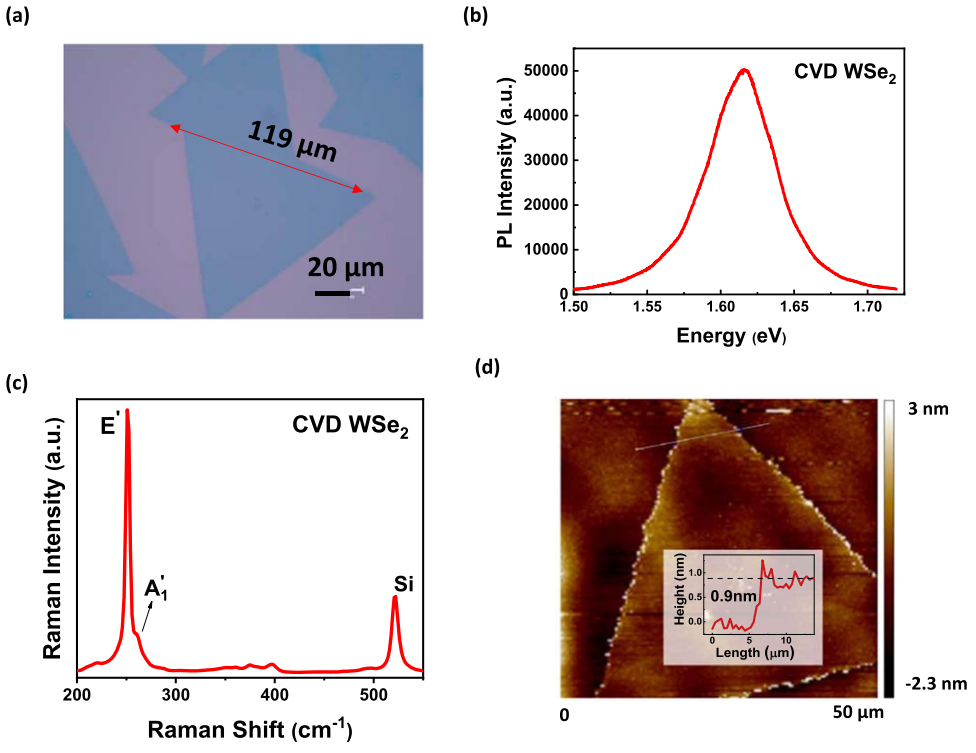

Figure 2. Microscopic characterization of monolayer WSe_2 grown by CVD. (a) Optical image, (b) Photoluminescence spectrum, (c) Raman spectrum, and (d) AFM image. The AFM height profile of the monolayer WSe_2 is shown in the inset of (d).

2.2. $MoSe_2/WSe_2$ and WSe_2/MoS_2 lateral heterostructures

Based on the MoS_2 and WSe_2 processes we developed, we further explored the synthesis of lateral heterostructures based on these materials via a two-step CVD process. Lateral $MoSe_2/WSe_2$ and WSe_2/MoS_2 heterostructures were successfully synthesized. For the $MoSe_2/WSe_2$ heterostructure, we first synthesized monolayer MoS_2 using MoO_3 and sulfur precursors at 730 °C for 5 min. Then we loaded the MoS_2 samples to the single-zone furnace with WO_3 and selenium precursors and grew WSe_2 at 875 °C for 6 min. Interestingly, we

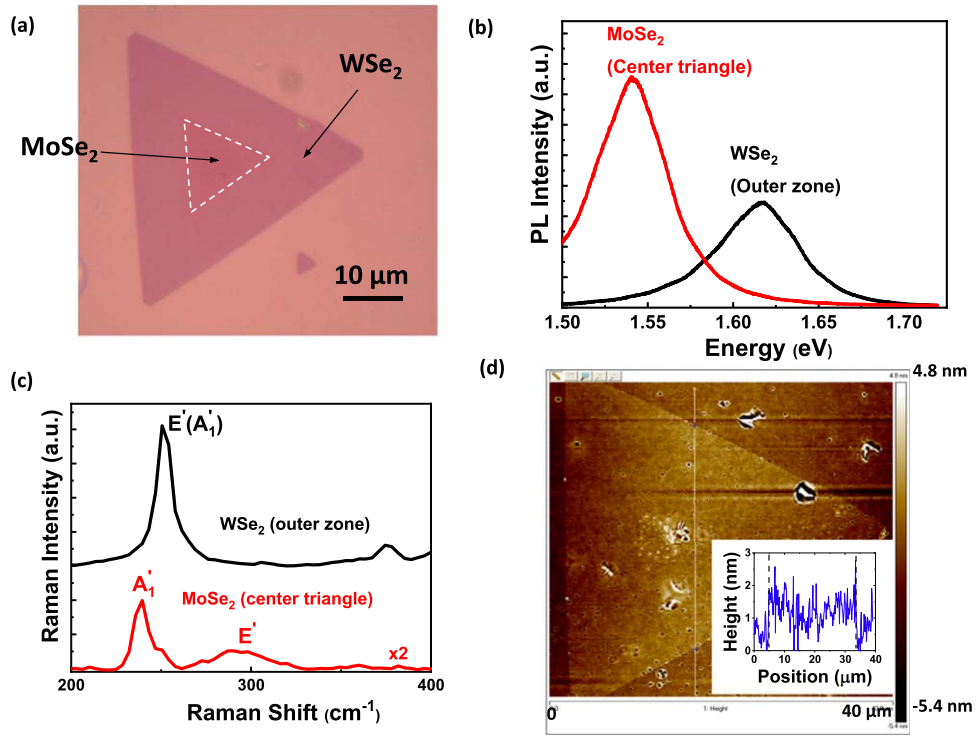

Figure 3. Lateral $MoSe_2/WSe_2$ heterostructure grown using a two-step CVD process with ion-exchange. (a) Optical image of the $MoSe_2/WSe_2$ heterostructure. (b) Photoluminescence spectra and (c) Raman spectra of the $MoSe_2$ located at center region of the triangle and WSe_2 located at the outer zone of the triangle. (d) AFM image of the heterostructure, with the height profile of the heterostructure shown in the inset.

found that $MoSe_2/WSe_2$ lateral structures were formed with $MoSe_2$ located at the center of the triangle, while WSe_2 located at the outer zone of the triangle. We suspect that during the WSe_2 growth, a Se–S ion exchange occurs in the MoS_2 region [37], converting the MoS_2 into $MoSe_2$. The optical image, photoluminescence spectra, and Raman spectra of the heterostructures are shown in figures 3(a)–(c), respectively. From the PL spectra, we can see that the PL spectrum taken at the center of the triangle has a peak at ~1.54 eV, which corresponds to the bandgap of monolayer $MoSe_2$ [38, 39], while the PL taken at the outer zone of the triangle has a peak at ~1.62 eV, which corresponds to the bandgap of monolayer WSe_2. The Raman spectra further confirmed that the heterostructure is $MoSe_2/WSe_2$. The Raman spectrum taken at the inner triangle of the heterostructure shows two peaks located at 239.5 and 287.2 cm^{-1}, corresponding to A_1' and E' modes in monolayer $MoSe_2$ respectively [27, 40], while the Raman spectrum taken at the outer zone shows one peak at 250.5 cm^{-1}, corresponding to E' (A_1') of the monolayer WSe_2. The atomic force microscopy (AFM) image and the line profile for the heterostructure are shown in figure 3(d) and its inset. No clear step feature is observed across the boundary between $MoSe_2$ and WSe_2, which confirms that it is a lateral heterostructure.

For WSe_2/MoS_2 heterostructures, WSe_2 was grown first using WO_3 and selenium precursors at 875 °C, followed by MoS_2 growth using MoO_3 and sulfur precursors at 730 °C. In contrast to the previous case, no ion-exchange was observed and lateral WSe_2/MoS_2 heterostructures were formed. The optical image, photoluminescence spectra, Raman spectra, AFM image and height profile of the WSe_2/MoS_2 heterostructure are all shown in figures 4(a)–(e). From the PL spectra, we can see that the bandgap of the material in the inner triangle is 1.62 eV, corresponding to monolayer WSe_2, while the bandgap of the material at the outer zone is 1.85 eV, corresponding to monolayer MoS_2. The Raman spectrum and AFM profile further confirmed that it is a monolayer WSe_2/MoS_2 lateral heterostructure. These results indicate that the sequence of the growth temperature in the two-step CVD process plays an important role in the heterostructure composition. If a low-temperature growth is followed by a high-temperature growth, ion-exchange can occur and the initial TMDC layer may be converted to a new material. In the meantime, the second material is grown laterally from the edge of the first material. If a high-temperature process is followed by a low temperature process, the TMDC grown in the first step may be stable enough to endure the grown conditions in second step and the second material will just epitaxially extend from the edges. These findings provide new insights into the growth of lateral heterostructures, especially through ion-exchange. As compared to the one-step process [18, 19], this two-step process can potentially provide better control on the size of each material, as well as sharper interface in the

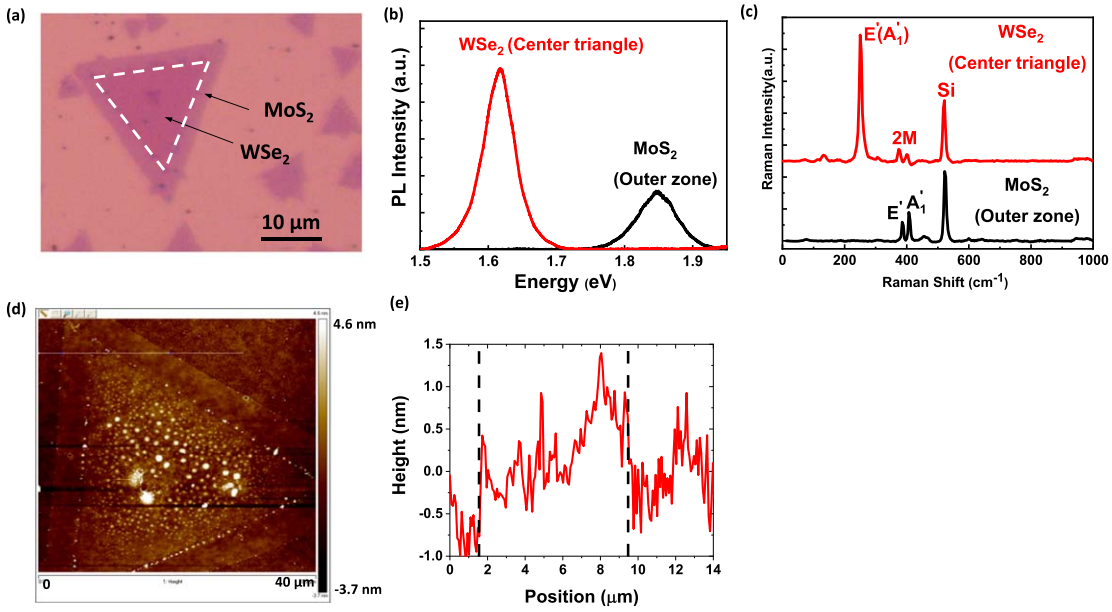

Figure 4. Lateral WSe_2/MoS_2 heterostructures grown via a two-step CVD process. (a) Optical image of the heterostructure, (b) photoluminescence spectra and (c) Raman spectra of the WSe_2 located at center region of the triangle and MoS_2 located at the outer zone of the triangle. (d) AFM image of the heterostructure. (e) AFM height profile of the heterostructure.

lateral heterostructures [23]. In addition, this synthesis method can further be expanded into multiple steps with various materials, which can enable the formation of lateral superlattices.

3. CVD MoS_2 and WSe_2 on sapphire substrates

In the past, most TMDCs were synthesized on SiO_2/Si substrates, since the SiO_2 layer can enhance the visibility of the monolayer 2D TMDCs and in the meantime serves as the back-gate dielectric in the electronic devices. However, the TMDCs grown on SiO_2/Si substrates are typically random in orientation, due to the amorphous nature of SiO_2. It was discovered recently that crystalline substrates such as sapphire can facilitate aligned growth of TMDCs through van der Waal interaction [41–43]. This can greatly reduce the number of grain boundaries of the TMDCs when these islands merge together to form a continuous film. In this project, we investigated the synthesis of MoS_2 and WSe_2 on sapphire substrate. C-plane sapphire was used as the substrate. The growth condition for MoS_2 on sapphire is similar to that on the SiO_2/Si substrate, except that the growth temperature is reduced to 710 °C. Figure 5(a) shows an optical image of the MoS_2 synthesized on sapphire. The statistic of the domain edges of this sample is shown in figure 5(b). We can see that most domain edges of the MoS_2 are oriented along the dominant directions (0°, 60° and 120°). This result indicates that the C-plane sapphire substrate effectively facilitated the alignment of the MoS_2 domains. This result is consistent with the previous reports [44, 45]. The MoS_2 domain size is ~10 μm. Raman, PL and AFM of these MoS_2 films are shown in figures 5(c)–(e). The PLs of the MoS_2 and the sapphire substrate without MoS_2 are shown in figure 5(b). A PL peak at 1.83 eV is observed, indicating the MoS_2 film is monolayer. The PL peak at 1.78 eV is attributed to the C-plane sapphire [45], which is also observed in the PL spectrum of the sapphire substrate without MoS_2. Raman spectra of the MoS_2 and the sapphire substrate are plotted side-by-side in figure 5(c). The Raman spectrum of MoS_2 on sapphire substrate shows peaks at 385 and 406 cm^{-1}, which correspond to E' and A_1' modes in MoS_2, and a peak at 417 cm^{-1}, which belongs to the sapphire A_{1g} mode. The AFM measurement further confirmed that the MoS_2 film is monolayer.

In addition to MoS_2, we also investigated the synthesis of WSe_2 on sapphire substrates. We used growth conditions similar to those for WSe_2 grown on SiO_2/Si substrate. A large number of WSe_2 triangles with large domains (~50 μm) were observed on the sapphire substrates. The optical image and the statistic of the domain edges of the WSe_2 on sapphire are shown in figures 6(a) and (b). As compared to MoS_2 on sapphire substrate, WSe_2 on sapphire is less aligned. The random orientation of WSe_2 on sapphire substrates is also observed previously [46]. This can be explained by the different growth temperature for MoS_2 and WSe_2. In our experiment, WSe_2 is grown at 875 °C, while MoS_2 is grown at a lower temperature 710 °C. Based on the density function theory (DFT) calculation, the fluctuation of the binding energy between the sapphire substrate and MoS_2 associated with varying orientations is very small (~71 meV) [45]. If we assume that the fluctuation of

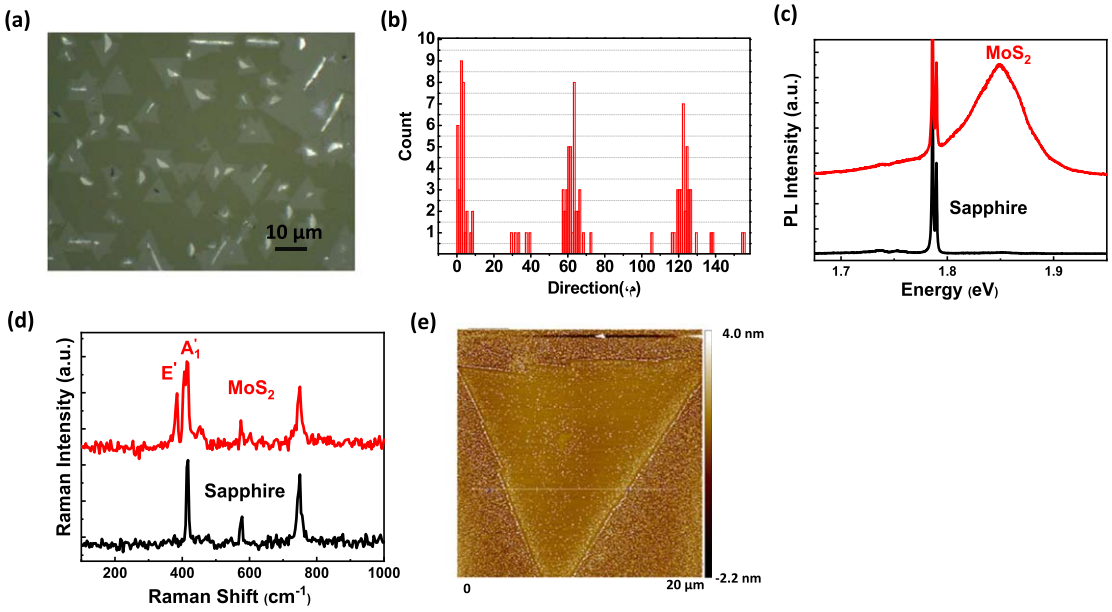

Figure 5. CVD MoS_2 grown on sapphire substrate. (a) Optical image of the CVD MoS_2 grown on sapphire substrate. (b) Statistics of the domain orientations for the sample shown in (a). (c) Photoluminescence spectra, and (d) Raman spectra of the MoS_2 and the sapphire substrate. (e) AFM image of the CVD MoS_2 grown on sapphire substrate.

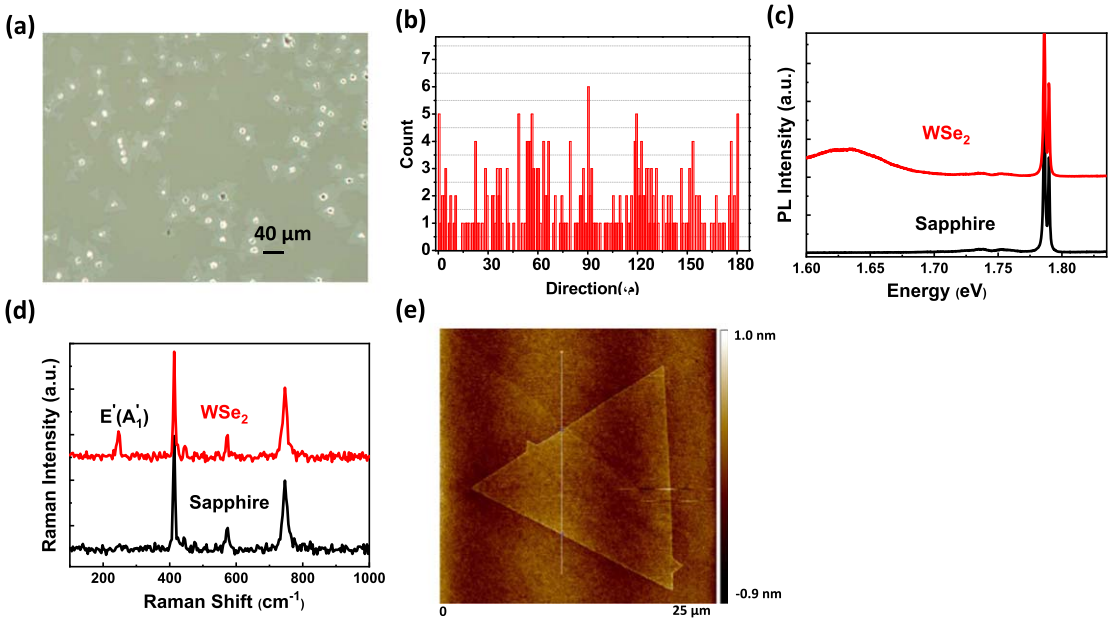

Figure 6. CVD WSe_2 grown on sapphire substrate. (a) Optical image of the CVD WSe_2 grown on sapphire substrate. (b) Statistics of the domain directions for the sample shown in (a). (c) Photoluminescence spectra, and (d) Raman spectra of the WSe_2 and the sapphire substrate. (e) AFM image of the CVD WSe_2 grown on sapphire substrate.

binding energy between WSe_2 and the sapphire substrate is also very small, similar to the case in MoS_2, then at high growth temperatures, the energy barrier between different orientations can be lower than the thermal energy ($k_BT \sim 100$ meV at 850 °C). This high thermal energy could smear out the binding energy difference for various orientation angles, which results in random orientation in the synthesized WSe_2 triangles. Raman and PL spectra of WSe_2 on sapphire substrates are shown in figures 6(c) and (d). The PL peak at 1.63 eV is observed, indicating that the film is monolayer WSe_2. Raman peaks at 246.2 cm^{-1} correspond to E' and A_1' vibrational modes in monolayer WSe_2. The AFM measurement show the equilateral triangle with a step height of ~0.5 nm, shown in figure 6(e), further confirming the monolayer nature of the WSe_2 film.

4. Conclusions

In summary, we systematically investigated the CVD synthesis of transitional metal dichalcogenides and their heterostructures. Monolayer MoS_2 and WSe_2 with domain sizes up to 100 μm were synthesized on SiO_2/Si substrates. Lateral heterostructures of monolayer $MoSe_2/WSe_2$ and WSe_2/MoS_2 were formed using a two-step process. We found that if MoS_2 growth is followed by WSe_2 growth, the MoS_2 layer would be converted into $MoSe_2$ and a lateral $MoSe_2/WSe_2$ heterostructure would be formed, possibly because the growth temperature for WSe_2 (875 °C) is much higher than that for MoS_2 (730 °C). At this high temperature, the sulfur atoms become unstable and are replaced by selenium atoms. To the best of our knowledge, this is the first report of lateral $MoSe_2/WSe_2$ heterostructures synthesized by the atom interchange method. We also found that if WSe_2 was synthesized followed by MoS_2 growth, no atom interchange was observed and lateral WSe_2/MoS_2 heterostructures were formed. In addition, we also investigated the synthesis of MoS_2 and WSe_2 on sapphire substrates. We found that most MoS_2 domain edges are aligned with the primary directions, while the WSe_2 domain edges are mostly randomly oriented. These TMDC materials and their heterostructures have high potential in large-scale growth and will have broad applications in nanoscale electronics and photonic devices.

Acknowledgments

The authors would like to acknowledge the support from the Office of Naval Research (ONR) under Grant NAVY N00014-17-1-2973.

ORCID iDs

Yuhang Cai https://orcid.org/0000-0002-6278-204X
Wenjuan Zhu https://orcid.org/0000-0003-2824-1386

References

[1] Britnell L *et al* 2013 Strong light–matter interactions in heterostructures of atomically thin films *Science* **340** 1311–4
[2] Fang H *et al* 2014 Strong interlayer coupling in van der Waals heterostructures built from single-layer chalcogenides *P. Natl. Acad. Sci. USA* **111** 6198–202
[3] Furchi M M, Pospischil A, Libisch F, Burgdorfer J and Mueller T 2014 Photovoltaic effect in an electrically tunable van der waals heterojunction *Nano Lett.* **14** 4785–91
[4] Nitta J, Akazaki T, Takayanagi H and Enoki T 1997 Gate control of spin–orbit interaction in an inverted In(0.53)Ga(0.47)AS/In(0.52)Al(0.48)AS heterostructure *Phys. Rev. Lett.* **78** 1335–8
[5] Nourbakhsh A, Zubair A, Dresselhaus M S and Palacios T 2016 Transport properties of a MoS_2/WSe_2 heterojunction transistor and its potential for application *Nano Lett.* **16** 1359–66
[6] Roy T, Tosun M, Cao X, Fang H, Lien D H, Zhao P D, Chen Y Z, Chueh Y L, Guo J and Javey A 2015 Dual-gated MoS_2/WSe_2 van der Waals tunnel diodes and transistors *Acs Nano* **9** 2071–9
[7] Roy T, Tosun M, Kang J S, Sachid A B, Desai S B, Hettick M, Hu C M C and Javey A 2014 Field-effect transistors built from all two-dimensional material components *Acs Nano* **8** 6259–64
[8] Tsai M L, Su S H, Chang J K, Tsai D S, Chen C H, Wu C I, Li L J, Chen L J and He J H 2014 Monolayer MoS_2 heterojunction solar cells *Acs Nano* **8** 8317–22
[9] Withers F *et al* 2015 Light-emitting diodes by band-structure engineering in van der Waals heterostructures *Nat. Mater.* **14** 301–6
[10] Rigos A F, Hill H M, Li Y L, Chernikov A and Heinz T F 2015 Probing interlayer interactions in transition metal dichalcogenide heterostructures by optical spectroscopy: MoS_2/WS_2 and $MoSe_2/WSe_2$ *Nano Lett.* **15** 5033–8
[11] Chiu M H, Zhang C D, Shiu H W, Chuu C P, Chen C H, Chang C Y S, Chen C H, Chou M Y, Shih C K and Li L J 2015 Determination of band alignment in the single-layer MoS_2/WSe_2 heterojunction *Nat. Commun.* **6** 7666
[12] Hanbicki A T, Chuang H J, Rosenberger M R, Hellberg C S, Sivaram S V, McCreary K M, Mazin I I and Jonker B T 2018 Double indirect interlayer exciton in a $MoSe_2/WSe_2$ van der Waals heterostructure *Acs Nano* **12** 4719–26
[13] Wang K *et al* 2016 Interlayer coupling in twisted WSe_2/WS_2 bilayer heterostructures revealed by optical spectroscopy *Acs Nano* **10** 6612–22
[14] Yuan J T, Najmaei S, Zhang Z H, Zhang J, Lei S D, Ajayan P M, Yakobson B I and Lou J 2015 Photoluminescence quenching and charge transfer in artificial heterostacks of monolayer transition metal dichalcogenides and few-layer black phosphorus *Acs Nano* **9** 555–63
[15] Nayak P K *et al* 2017 Probing evolution of twist-angle-dependent interlayer excitons in $MoSe_2/WSe_2$ van der Waals heterostructures (vol 11, pg 4041, 2017) *Acs Nano* **11** 9566–9566
[16] Tongay S *et al* Tuning interlayer coupling in large-area heterostructures with CVD-grown MoS_2 and WS_2 monolayers *Nano Lett.* 2014 **14** 3185–90
[17] Hong X P, Kim J, Shi S F, Zhang Y, Jin C H, Sun Y H, Tongay S, Wu J Q, Zhang Y F and Wang F 2014 Ultrafast charge transfer in atomically thin MoS_2/WS_2 heterostructures *Nat. Nanotechnol.* **9** 682–6
[18] Huang C M, Wu S F, Sanchez A M, Peters J J P, Beanland R, Ross J S, Rivera P, Yao W, Cobden D H and Xu X D 2014 Lateral heterojunctions within monolayer $MoSe_2$-WSe_2 semiconductors *Nat. Mater.* **13** 1096–101
[19] Gong Y J *et al* 2014 Vertical and in-plane heterostructures from WS_2/MoS_2 monolayers *Nat. Mater.* **13** 1135–42
[20] Li M Y *et al* 2015 Epitaxial growth of a monolayer WSe_2-MoS_2 lateral p-n junction with an atomically sharp interface *Science* **349** 524–8

[21] Yu Y *et al* 2015 Equally efficient interlayer exciton relaxation and improved absorption in epitaxial and nonepitaxial MoS_2/WS_2 heterostructures *Nano Lett.* **15** 486–91
[22] Zhang X Q, Lin C H, Tseng Y W, Huang K H and Lee Y H 2015 Synthesis of lateral heterostructures of semiconducting atomic layers *Nano Lett.* **15** 410–5
[23] Gong Y J *et al* 2015 Two-step growth of two-dimensional $WSe_2/MoSe_2$ heterostructures *Nano Lett.* **15** 6135–41
[24] Mak K F, Lee C, Hone J, Shan J and Heinz T F 2010 Atomically thin MoS_2: a new direct-gap semiconductor *Phys. Rev. Lett.* **105** 136805
[25] Splendiani A, Sun L, Zhang Y B, Li T S, Kim J, Chim C Y, Galli G and Wang F 2010 Emerging photoluminescence in monolayer MoS_2 *Nano Lett.* **10** 1271–5
[26] Wang Q H, Kalantar-Zadeh K, Kis A, Coleman J N and Strano M S 2012 Electronics and optoelectronics of two-dimensional transition metal dichalcogenides *Nat. Nanotechnol.* **7** 699–712
[27] Zhang X, Qiao X F, Shi W, Wu J B, Jiang D S and Tan P H 2015 Phonon and Raman scattering of two-dimensional transition metal dichalcogenides from monolayer, multilayer to bulk material *Chem. Soc. Rev.* **44** 2757–85
[28] Zeng H L *et al* 2013 Optical signature of symmetry variations and spin-valley coupling in atomically thin tungsten dichalcogenides *Sci. Rep-Uk* **3** 1608
[29] Liu B L, Fathi M, Chen L, Abbas A, Ma Y Q and Zhou C W 2015 Chemical vapor deposition growth of monolayer WSe_2 with tunable device characteristics and growth mechanism study *Acs Nano* **9** 6119–27
[30] Clark G, Wu S F, Rivera P, Finney J, Nguyen P, Cobden D H and Xu X D 2014 Vapor-transport growth of high optical quality WSe_2 monolayers *Apl. Materials* **2** 101101
[31] Ross J S *et al* 2014 Electrically tunable excitonic light-emitting diodes based on monolayer WSe_2 p-n junctions *Nat. Nanotechnol.* **9** 268–72
[32] Baugher B W H, Churchill H O H, Yang Y F and Jarillo-Herrero P 2014 Optoelectronic devices based on electrically tunable p-n diodes in a monolayer dichalcogenide *Nat. Nanotechnol.* **9** 262–7
[33] Pospischil A, Furchi M M and Mueller T 2014 Solar-energy conversion and light emission in an atomic monolayer p-n diode *Nat. Nanotechnol.* **9** 257–61
[34] Zhou H L *et al* 2015 Large area growth and electrical properties of p-Type WSe_2 atomic layers *Nano Lett.* **15** 709–13
[35] Huang J-K, Pu J, Hsu C-L, Chiu M-H, Juang Z-Y, Chang Y-H, Chang W-H, Iwasa Y, Takenobu T and Li L-J 2014 Large-area synthesis of highly crystalline WSe_2 monolayers and device applications *Acs Nano* **8** 923–30
[36] Tonndorf P *et al* 2013 Photoluminescence emission and Raman response of monolayer MoS_2, $MoSe_2$, and WSe_2 *Opt. Express* **21** 4908–16
[37] Lin Y C *et al* 2015 Atomically thin resonant tunnel diodes built from synthetic van der Waals heterostructures *Nat. Commun.* **6** 7311
[38] Tongay S, Zhou J, Ataca C, Lo K, Matthews T S, Li J B, Grossman J C and Wu J Q 2012 Thermally driven crossover from indirect toward direct bandgap in 2D semiconductors: $MoSe_2$ versus MoS_2 *Nano Lett.* **12** 5576–80
[39] Wen X W *et al* 2018 Ultrafast probes of electron-hole transitions between two atomic layers *Nat. Commun.* **9** 1859
[40] Wang X L *et al* 2014 Chemical vapor deposition growth of crystalline mono layer $MoSe_2$ *Acs Nano* **8** 5125–31
[41] Dumcenco D *et al* 2015 Large-area epitaxial monolayer MoS_2 *Acs Nano* **9** 4611–20
[42] Chen L, Liu B, Ge M, Ma Y, Abbas A N and Zhou C 2015 Step-edge-guided nucleation and growth of aligned WSe_2 on sapphire via a layer-over-layer growth mode *Acs Nano* **9** 8368–75
[43] Nakano M, Wang Y, Kashiwabara Y, Matsuoka H and Iwasa Y 2017 Layer-by-layer epitaxial growth of scalable WSe_2 on sapphire by molecular beam epitaxy *Nano Lett.* **17** 5595–9
[44] Dumcenco D *et al* 2015 Large-area epitaxial mono layer MoS_2 *Acs Nano* **9** 4611–20
[45] Ji Q Q, Kan M, Zhang Y, Guo Y, Ma D L, Shi J P, Sun Q, Chen Q, Zhang Y F and Liu Z F 2015 Unravelling orientation distribution and merging behavior of mono layer MoS_2 domains on sapphire *Nano Lett.* **15** 198–205
[46] Huang J K, Pu J, Hsu C L, Chiu M H, Juang Z Y, Chang Y H, Chang W H, Iwasa Y, Takenobu T and Li L J 2014 Large-area synthesis of highly crystalline WSe_2 mono layers and device applications *Acs Nano* **8** 923–30